Mass–Velocity Dispersion Relation in MaNGA Brightest Cluster Galaxies

Yong Tian[1] , Han Cheng[1], Stacy S. McGaugh[2] , Chung-Ming Ko[1,3,†] , and Yun-Hsin Hsu[4,5]
[1] Institute of Astronomy, National Central University, Taoyuan 32001, Taiwan; cmko@astro.ncu.edu.tw
[2] Department of Astronomy, Case Western Reserve University, 10900 Euclid Avenue, Cleveland, OH 44106, USA; stacy.mcgaugh@case.edu
[3] Department of Physics and Center for Complex Systems, National Central University, Taoyuan 32001, Taiwan
[4] Academia Sinica Institute of Astronomy and Astrophysics (ASIAA), No. 1, Section 4, Roosevelt Road, Taipei 10617, Taiwan
[5] Institute of Astronomy, National Tsing Hua University, No. 101, Section 2, Kuang-Fu Road, Hsinchu 30013, Taiwan
Received 2021 July 2; revised 2021 August 2; accepted 2021 August 3; published 2021 August 19

Abstract

We investigate a kinematic scaling relation between the baryonic mass and the flat velocity dispersion, i.e., mass–velocity dispersion relation (MVDR), from the brightest cluster galaxies (BCGs) to the galaxy clusters. In our studies, the baryonic mass of BCGs is mainly estimated by photometry. The velocity dispersion profiles are explored with the integrated field unit by Mapping Nearby Galaxies at Apache Point Observatory (MaNGA). For the first time, we reveal two significant results with 54 MaNGA BCGs: (1) the flat velocity dispersion profiles; (2) a tight empirical relation on the BCG-cluster scale together with cluster samples, i.e., MVDR, $\log(M_{bar}/M_{\odot}) = 4.1^{+0.1}_{-0.1} \log(\sigma_{los}/\mathrm{km\ s^{-1}}) + 1.6^{+0.3}_{-0.3}$, with a tiny lognormal intrinsic scatter of $10^{+2}_{-1}\%$. This slope is identical to the acceleration relation in galaxy clusters, which is reminiscent of the spiral galaxies, albeit at a larger characteristic acceleration scale. The residuals of the MVDR represent a Gaussian distribution, displaying no correlations with four properties: baryonic mass, scale length, surface density, and redshift. Notably, the MVDR on the BCG-cluster scale provides a strict test, which disfavors the general prediction of the slope of three in the dark matter model.

Unified Astronomy Thesaurus concepts: Galaxy kinematics (602); Brightest cluster galaxies (181); Giant elliptical galaxies (651); Galaxy clusters (584); Dark matter (353)

1. Introduction

A kinematic scaling relation is the counterpart of a dynamical scaling relation, which plays a major role in understanding fundamental physics. For examples, Kepler's law leads to Newtonian dynamics in the solar system. However, Kepler's law is no longer applicable in spiral galaxies, well-known as the dark matter (DM) problem. Instead, a different kinematic relation was discovered between the baryonic mass and the flat rotation velocity, called the baryonic Tully–Fisher relation (BTFR; McGaugh et al. 2000; Verheijen 2001; McGaugh 2011; Lelli et al. 2016, 2019). Similarly in elliptical galaxies and galaxy clusters, such a correlation was found between the baryonic mass and the velocity dispersion, called the baryonic Faber–Jackson relation (BFJR; Sanders 2010; Famaey & McGaugh 2012).

In galaxies, the BTFR and the BFJR can be implied by the radial acceleration relation (RAR) in the low acceleration approximation. Not long ago, McGaugh et al. (2016) explored a tight correlation between the observed acceleration $g_{obs} = |\partial\Phi_{obs}/\partial r| = v^2/r$ and the baryonic acceleration $g_{bar} = GM_{bar}(<r)/r^2$ as

$$g_{obs} \simeq \sqrt{g_{bar}g_{\dagger}}, \qquad (1)$$

with an acceleration scale $g_{\dagger} = (1.20 \pm 0.02) \times 10^{-10}\ \mathrm{m\ s^{-2}}$. In addition, the RAR implied $v^4 = GM_{bar}g_{\dagger}$ for the BTFR and $\sigma^4 \simeq GM_{bar}g_{\dagger}$ for the BFJR (Lelli et al. 2017; McGaugh 2020; Milgrom 2020). Particularly, those correlations were clearly described in Modified Newtonian Dynamics (MOND; Milgrom 1983) about four decades ago. Furthermore, MOND has been tested in gravitational lensing effects (Tian et al. 2009; Tian & Ko 2019; Brouwer et al. 2021). However, MOND found a residual missing mass in galaxy clusters (Sanders 2003;

Famaey & McGaugh 2012), which questioned the validity of the RAR on the cluster scale.

Recently, Tian et al. (2020) investigated the existence of a radial acceleration relation on cluster scales using the Cluster Lensing and Supernova survey with Hubble (CLASH; Postman et al. 2012). In the CLASH sample, g_{obs} was measured by strong-lensing, weak-lensing shear-and-magnification data (Umetsu et al. 2016), while g_{bar} was calculated with X-ray data sets (Donahue et al. 2014) plus the estimated stellar mass from the empirical gas fraction (Chiu et al. 2018). The result is a parallel RAR (CLASH RAR):

$$g_{obs} \simeq \sqrt{g_{bar}g_{\ddagger}}, \qquad (2)$$

with a larger acceleration scale $g_{\ddagger} = (2.0 \pm 0.1) \times 10^{-9}\ \mathrm{m\ s^{-2}}$ than observed in rotating galaxies. The CLASH RAR is a tight correlation with a small intrinsic scatter $\sigma_{int} = 15\%$. Other works also demonstrate a similar acceleration scale in galaxy clusters (Pradyumna et al. 2021).

While supposing the validity of the CLASH RAR in dynamics, one can derive a mass–velocity dispersion relation (MVDR), $\sigma^4 \simeq GM_{bar}g_{\ddagger}$, on the brightest cluster galaxy (BCG)-cluster scale. Moreover, its implications include a flat velocity dispersion profile in both BCGs and clusters. This similarity is reminiscent of the RAR in galaxies, albeit with a larger acceleration scale $g_{\ddagger}$.

Recently, Tian et al. (2021) have quantified the MVDR with 29 galaxy clusters in the HIghest X-ray FLUx Galaxy Cluster Sample (HIFLUGCS). In their studies, the baryonic mass was dominated by X-ray gas (Zhang et al. 2011) plus the stellar mass estimated on the scaling relation (Giodini et al. 2009). All 29 HIFLUGCS clusters illustrated a flat tail in the line-of-sight (los) velocity dispersion profile. By Bayesian statistics, Tian et al. (2021) have

---

† Corresponding author.

obtained the MVDR in the galaxy cluster as

$$\log\left(\frac{M_{\rm bar}}{M_\odot}\right) = 4.1^{+0.4}_{-0.4} \log\left(\frac{\sigma_{\rm los}}{{\rm km\,s^{-1}}}\right) + 1.6^{+1.0}_{-1.3}, \qquad (3)$$

with a small intrinsic scatter of $\sigma_{\rm int} = 12^{+3}_{-3}\%$. In addition, this intercept implied a consistent acceleration scale $g_\ddagger$ of the CLASH RAR. Consequently, the success of an MVDR in galaxy clusters raises the same issue in BCGs.

Although the kinematic scaling relations were widely studied in BCGs such as the Faber–Jackson relation and the fundamental plane (e.g., see Oegerle & Hoessel 1991; Zaritsky et al. 2006; Bernardi et al. 2007; Samir et al. 2020), it has never been clear if there is continuity in a single MVDR from the scale of individual BCGs to clusters of galaxies (Sanders 1994). As for the flat profiles of BCGs, it has been a lack of systematic studies of the velocity dispersion profiles. Besides, there is only one BCG per cluster, and sufficiently sensitive, spatially resolved observations have been rare until now.

In this work, we investigate the MVDR with 54 Mapping Nearby Galaxies at Apache Point Observatory (MaNGA) BCGs and compare them with 29 HIFLUGCS clusters. The paper is organized as follows. In Section 2, we introduce the data in the MaNGA BCG sample and the method to analyze the velocity dispersion profile. In Section 3, we inspect the MVDR on the BCG-cluster scale by Bayesian statistics and calculate the residuals against four galaxy-cluster properties. In Section 4, we discuss our results with the consistency of the CLASH RAR and the implications for the dark matter problems. Finally, we summarize our work in Section 5. Throughout this paper, we assume a flat Λ cold dark matter (ΛCDM) cosmology with $\Omega_{\rm m} = 0.3$, $\Omega_\Lambda = 0.7$, and a Hubble constant of $H_0 = 70\ {\rm km\,s^{-1}\,Mpc^{-1}}$.

2. Data and Methods

To study the MVDR in BCGs, we estimated the baryonic mass and analyzed their velocity dispersion profiles at the outermost radius. The baryonic mass is composed of the stellar mass and the gas mass of BCGs. Since BCGs are elliptical galaxies, stars are usually concentrated in their center. So, it is difficult to measure their velocity far from the center.

Investigating the internal kinematics structure has motivated some observations with integrated field units (IFUs), which employed spatially resolved spectroscopy. Among them, MaNGA is the largest survey targeted with an unprecedented sample of 10,000 nearby galaxies (Bundy et al. 2015).

In this work, we exploited BCGs in public MaNGA Product Lunch-6 (MPL-6), which contained a total number of 4824 currently. This data set corresponds to SDSS Data Release Fifteen (DR15; Aguado et al. 2019). By combining both data of DR15 and MPL-6, we got sufficient information of the baryonic mass and internal kinematics profile for this work.

2.1. BCG Samples

Because BCGs are the brightest galaxies usually positioned at the center of a galaxy cluster, they can be identified by given memberships. The BCG samples of SDSS has been systematically explored in Yang et al. (2007). They obtained lots of groups by developing the halo-based group finder in Data Release Seventh

Table 1
Properties of 54 MaNGA BCGs

Plateifu	z[a]	$\log(M_{\rm bar})$[b] $(M_\odot)$	$\sigma_{\rm los}$[c] $({\rm km\,s^{-1}})$
8625-12704*	0.027	11.541 ± 0.077	298 ± 5
9181-12702*	0.041	11.622 ± 0.086	266 ± 10
9492-9101	0.053	11.785 ± 0.085	291 ± 10
8258-3703	0.059	11.246 ± 0.096	190 ± 17
8331-12701	0.061	11.231 ± 0.086	195 ± 11
8600-12703*	0.061	11.332 ± 0.086	220 ± 11
8977-3703*	0.074	11.475 ± 0.086	246 ± 9
8591-3704	0.075	11.506 ± 0.106	281 ± 9
8591-6102	0.076	11.435 ± 0.089	262 ± 13
8335-6103	0.082	11.575 ± 0.086	313 ± 13
9888-12703	0.083	11.542 ± 0.089	300 ± 12
9043-3704*	0.084	11.473 ± 0.091	226 ± 10
9042-3702	0.084	11.050 ± 0.604	251 ± 18
8943-9102*	0.085	11.442 ± 0.087	135 ± 33
8613-6102	0.086	11.807 ± 0.083	331 ± 7
9002-3703	0.088	11.171 ± 0.092	203 ± 11
8939-6104	0.088	11.309 ± 0.086	271 ± 32
8455-12703*	0.092	11.559 ± 0.091	206 ± 9
9025-9101	0.096	11.813 ± 0.077	277 ± 24
8239-6103	0.097	11.361 ± 0.088	236 ± 32
9486-6103	0.098	11.401 ± 0.078	241 ± 5
8613-12705	0.099	12.029 ± 0.120	377 ± 129
9000-9101	0.105	11.225 ± 0.088	202 ± 10
8447-3702	0.109	11.596 ± 0.106	250 ± 19
9891-9101	0.111	11.609 ± 0.101	261 ± 16
8466-6104	0.113	11.552 ± 0.087	210 ± 14
9891-3701	0.114	11.462 ± 0.091	212 ± 5
8081-3701	0.115	11.556 ± 0.094	281 ± 9
9044-12703	0.117	11.414 ± 0.620	316 ± 10
8131-3703	0.119	11.592 ± 0.084	272 ± 27
9891-12701	0.120	11.442 ± 0.095	323 ± 67
9085-6102	0.120	11.702 ± 0.092	307 ± 13
9506-6103*	0.120	11.578 ± 0.087	297 ± 13
8943-3704	0.124	11.697 ± 0.082	266 ± 34
9490-9102	0.125	11.619 ± 0.088	278 ± 14
9043-9101	0.127	11.582 ± 0.092	336 ± 35
8725-12704	0.129	12.068 ± 0.086	504 ± 56
8989-12704	0.129	11.758 ± 0.094	285 ± 39
8989-12703	0.130	11.644 ± 0.124	279 ± 24
8728-3703	0.131	11.596 ± 0.090	226 ± 23
9865-12703	0.131	11.498 ± 0.083	211 ± 8
8717-1901	0.131	11.493 ± 0.081	268 ± 3
8991-6102	0.133	11.654 ± 0.099	270 ± 7
8555-3702	0.133	11.457 ± 0.089	240 ± 19
8554-6103	0.133	11.594 ± 0.088	297 ± 57
8995-6103	0.133	11.458 ± 0.096	208 ± 19
8720-12705	0.135	11.236 ± 0.096	228 ± 51
8615-12704	0.135	11.572 ± 0.081	471 ± 95
8554-6102	0.136	11.775 ± 0.115	304 ± 12
8616-12703	0.138	11.884 ± 0.089	308 ± 11
8616-3702	0.138	11.581 ± 0.089	284 ± 13
8247-9102*	0.140	11.734 ± 0.084	330 ± 24
9888-6104	0.147	11.729 ± 0.087	265 ± 6
8725-6104	0.148	11.614 ± 0.083	270 ± 38

Notes.
[a] Redshifts are from MaNGA Pipe3D.
[b] The baryonic mass including total stellar mass estimated by model photometry in SDSS DR15 and the measured gas mass in MaNGA marked with ∗ on the plateifu ID.
[c] The flat los velocity dispersion from MaNGA IFU in this work.
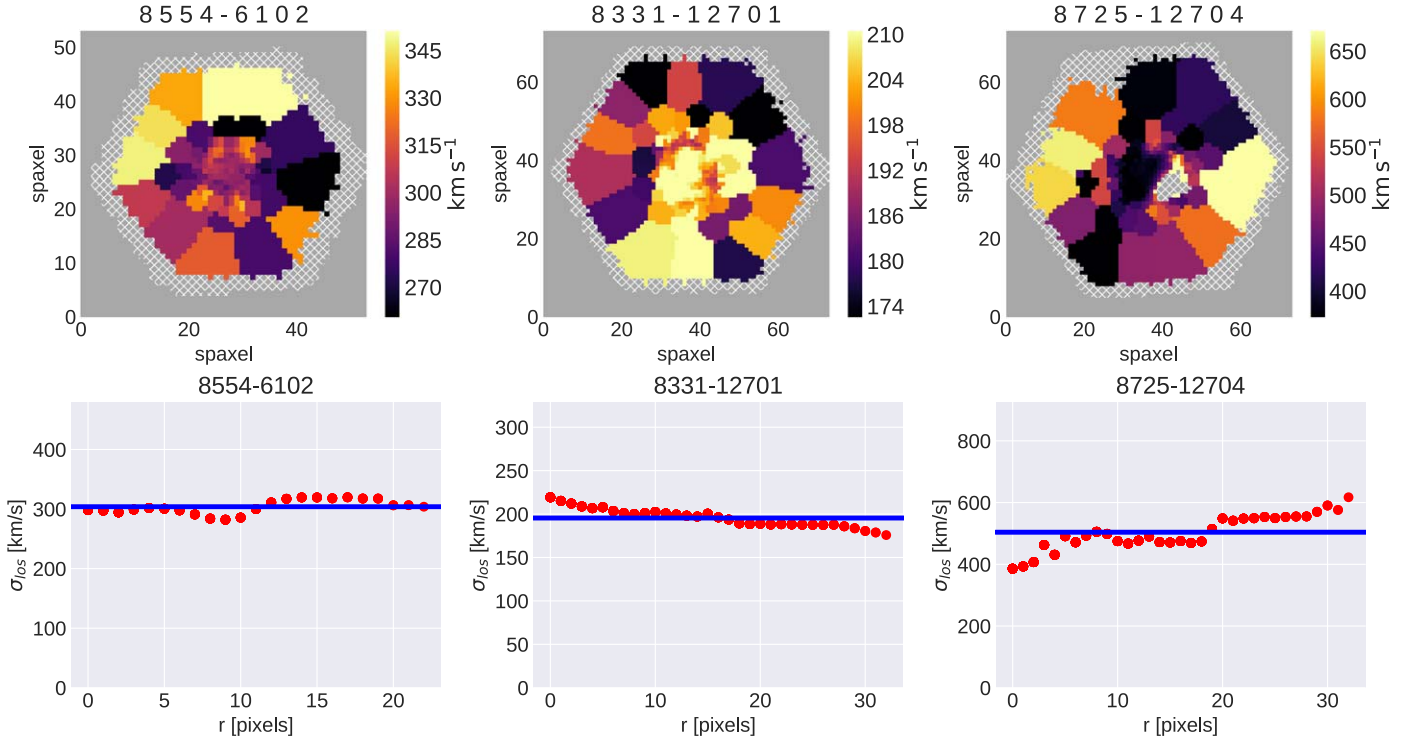
Figure 1. Three examples of MaNGA BCGs with the plateifu of "8554-6102," "8331-12701," and "8725-12704." Upper panel: the map plot of `Spaxel` data for the stellar velocity dispersion. Lower panel: velocity dispersion profiles in terms of radius. The red circles represent the los velocity dispersion of concentric circles at different radii. The blue solid lines represent the mean of the red data points, which is adopted as the flat los velocity dispersion of each BCG.

(DR7). When matching Yang's catalog with MPL-6, 73 samples in MaNGA were reidentified as BCGs by the color–magnitude and the membership distribution diagrams. In total, we got 76 BCGs when including three additional samples labeled by MaNGA.

In our studies, both complete spectra and IFU measurements are necessary for calculating the baryonic mass and the flat velocity dispersion. Among the samples, 6 lack sufficient MaNGA IFU data and 16 cases are without the SDSS spectra. Therefore, only 54 MaNGA BCGs meet the specific requirements of the MVDR. Their galactic properties are listed in Table 1, such as ID, redshift, baryonic mass M_{bar}, and the flat los velocity dispersion σ_{los}.

2.2. The Baryonic Mass

Because BCGs are usually elliptical galaxies, the baryonic mass is dominated by their stellar mass. The total stellar mass of 54 MaNGA BCGs can be estimated by model photometry in SDSS DR15. We adopt uncertainties that average over the occasional asymmetry in the photometric stellar mass estimates. The gas mass of BCGs is subdominant to stars. Only nine galaxies have measured gas masses in MaNGA (e.g., see the star marker ∗ of plateifu ID in Table 1), with the gas fraction in our samples ranging from 0.03% to 3.2% of the baryonic mass. Moreover, the hot gas contribution in the inner region (within the effective radius R_e) is insignificant compared to the stellar mass of BCG (e.g., Sartoris et al. 2020; Tian et al. 2020).

2.3. The Flat Velocity Dispersion

The flat los velocity dispersion of BCGs can be calculated by its one-dimensional profile relative to their centers. We apply `Marvin` developed in *Python* (Cherinka et al. 2019) to access

and analyze MaNGA `Spaxel` data for the los stellar velocity dispersion (Figure 1). All data below 20 km s^{-1} are discarded, because those are considered unreliable (Bundy et al. 2015; Durazo et al. 2018). We calculate the mean los velocity dispersion of each circle. We find the velocity dispersion profiles of BCGs to be remarkably flat. Only one BCG in our sample "8943-9102" exhibits a strongly declining profile. We therefore adopt the average σ_{los} as the characteristic value for each galaxy (blue lines in Figure 1).

3. Results

Our main goal is to explore the empirical kinematic scaling relation between two independent measurements in BCGs: the baryonic mass and the flat los velocity dispersion of stellar components. In addition to the tightness and the correlations among the galactic properties, we also study the intrinsic scatter and the residuals with Bayesian statistics. The relation and the residuals are elucidated in the following subsections.

3.1. MVDR with Bayesian Statistics

In the logarithmic plane of the MVDR, 54 MaNGA BCGs are distributed as a linear relation. We model them by introducing $y = mx + b$ with two independent variables: $y \equiv \ln(M_{bar}/M_\odot)$ and $x \equiv \ln(\sigma_{los}/\mathrm{km\ s^{-1}})$. With Bayesian statistics, we implement a Markov Chain Monte Carlo (MCMC) analysis with the orthogonal-distance-regression (ODR) method suggested in Lelli et al. (2019) and Tian et al. (2021).

The log-likelihood function is written as

$$-2\ln\mathcal{L} = \sum_i \ln(2\pi\sigma_i^2) + \sum_i \frac{\Delta_i^2}{\sigma_i^2}, \qquad (4)$$
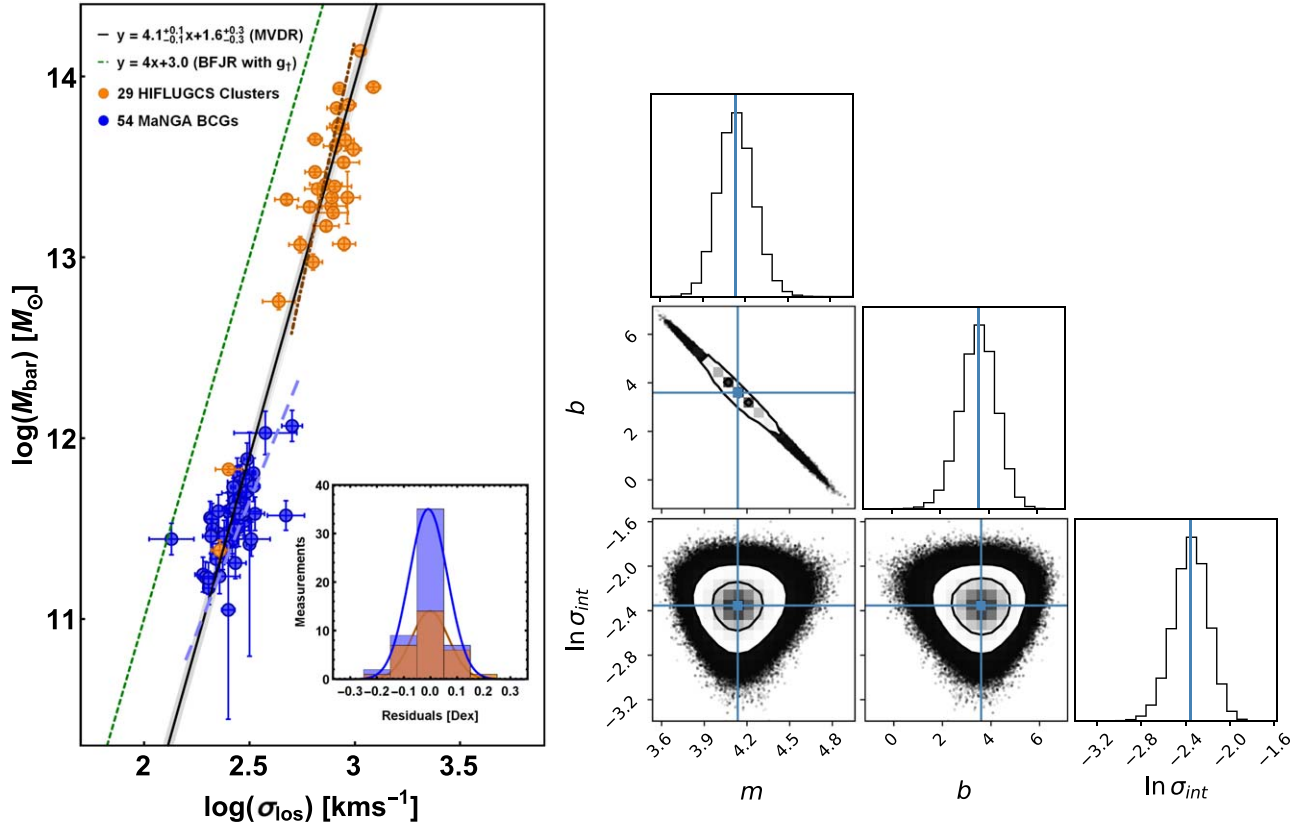
Figure 2. The MVDR of both BCGs and clusters. Left panel: the blue circles represent 54 MaNGA BCGs while the orange circles indicate 29 HIFLUGCS clusters in Tian et al. (2021). The black solid line represents the MVDR of all samples, $\log(M_{\mathrm{bar}}/M_\odot) = 4.1^{+0.1}_{-0.1} \log(\sigma_{\mathrm{los}}/\mathrm{km\ s}^{-1}) + 1.6^{+0.3}_{-0.3}$. The gray shaded area illustrates the 1σ error of the best fit. The inset panel demonstrates the histograms of the orthogonal residuals of both BCGs (blue) and clusters (orange). The histograms of both samples indicate Gaussian distributions with the same tiny half-width of 0.07 dex. The fitting results of a narrow dynamical range are illustrated with the brown dotted–dashed line for 27 HIFLUGCS clusters without the two smallest samples and the blue long dashed line for 54 MaNGA BCGs, respectively. The slopes of these lines are uncertain for lack of dynamic range; the BCG and cluster samples clearly connect when considered together. For comparison, the green dashed line demonstrates the BFJR with the acceleration scale of $g_\dagger$ assuming Jeans factor $J_\infty = 16$, $\log(M_{\mathrm{bar}}/M_\odot) = 4 \log(\sigma_{\mathrm{los}}/\mathrm{km\ s}^{-1}) + 3.0$. Right panel: triangle diagrams of the regression parameters for Equation (7) with marginalized one-dimensional (histograms) and two-dimensional posterior distributions. Black contours represent 1σ and 2σ confidence regions.

with

$$\Delta_i^2 = \frac{(y_i - m\,x_i - b)^2}{m^2 + 1}, \tag{5}$$

where i runs over all data points, and σ_i includes the observational uncertainties (σ_{x_i}, σ_{y_i}) and the lognormal intrinsic scatter σ_{int},

$$\sigma_i^2 = \frac{m^2 \sigma_{x_i}^2}{m^2 + 1} + \frac{\sigma_{y_i}^2}{m^2 + 1} + \sigma_{\mathrm{int}}^2. \tag{6}$$

We perform the ODR MCMC analysis for the slope and the intercept implemented in *Python* (*emcee*; Foreman-Mackey et al. 2013, 2019). While employing noninformative flat priors on the slope m and the intercept b within the interval of $[-100, 100]$, and the intrinsic scatter $\ln(\sigma_{\mathrm{int}}) \in [-5, 2]$, we discover a tighter correlation by

$$\log\left(\frac{M_{\mathrm{bar}}}{M_\odot}\right) = 4.1^{+0.1}_{-0.1} \log\left(\frac{\sigma_{\mathrm{los}}}{\mathrm{km\ s}^{-1}}\right) + 1.6^{+0.3}_{-0.3}, \tag{7}$$

with a tiny error of the lognormal intrinsic scatter of $10^{+2}_{-1}\%$. We present the regression parameters with the posteriors distribution in the right panel of Figure 2.

To justify the initial assumption of a Gaussian intrinsic scatter perpendicular to the fitting line, we examine the histogram of the orthogonal residuals Δ_i with respect to Equation (7) (see the inset panel of Figure 2). The distributions of the residuals demonstrate a Gaussian distribution with a tiny half-width (0.07 dex) for both BCGs and clusters.

To derive the precise value of the acceleration scale by the intercept, we apply a fixed slope ($m = 4$) and perform the ODR MCMC method again. It gives

$$\log\left(\frac{M_{\mathrm{bar}}}{M_\odot}\right) = 4 \log\left(\frac{\sigma_{\mathrm{los}}}{\mathrm{km\ s}^{-1}}\right) + 1.90^{+0.02}_{-0.02}, \tag{8}$$

with the same lognormal intrinsic scatter $\sigma_{\mathrm{int}} = 10^{+2}_{-1}\%$. Accordingly, the intercept implies an acceleration scale of $g_\ddagger = (0.9\text{–}2.4) \times 10^{-9}$ m s^{-2} by assuming Jeans factor $J_\infty \in [9, 25]$ (for details, see, e.g., Section 4.1 in Tian et al. 2021). This is consistent with that of the CLASH RAR, but larger than observed in spirals (McGaugh et al. 2016).

We also consider the fitting results of BCGs and clusters separately. Two distinct distributions can be divided as 54 MaNGA BCGs and 27 HIFLUGCS clusters. By implementing the same method, we get a different MVDR of BCGs with $m = 2.9^{+0.5}_{-0.3}$ and $b = 10.1^{+1.9}_{-2.6}$. In addition, the other case has been analyzed before: $m = 5.4^{+2.2}_{-1.1}$ and $b = -2.0^{+3.2}_{-6.3}$ (e.g., see
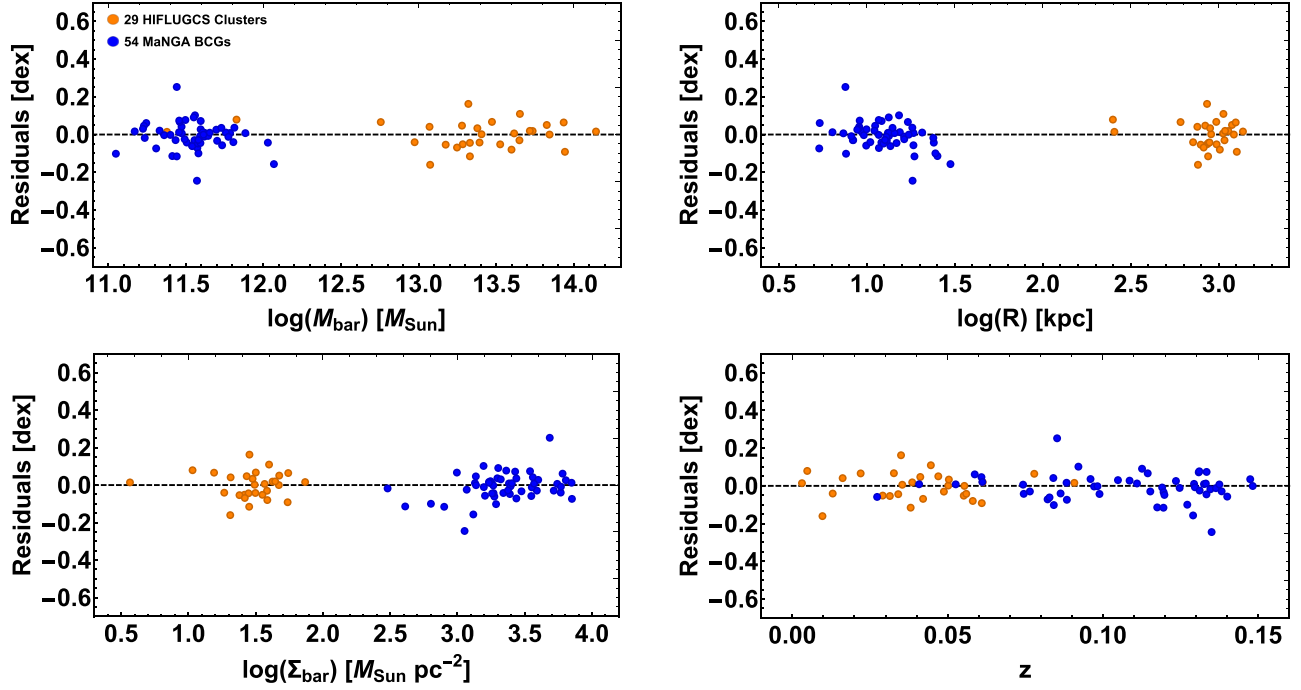
Figure 3. The orthogonal residuals after subtracting Equation (7) against four global quantities of galaxies and clusters: baryonic mass $M_{\rm bar}$ (upper left), scale length $R_{\rm e}$ for galaxies, r_{500} for clusters (upper right), baryonic mass surface density $\Sigma_{\rm bar}$ (lower left), and redshift (lower right). Blue circles denote BCGs and orange circles denote clusters. The dashed line represents zero difference.

the Section 3.1 in Tian et al. 2021). Two results are illustrated with the blue dashed and the brown dotted–dashed lines in Figure 2, respectively. Conversely, the uncertainty of the slopes and intercepts are much larger than the full samples due to the narrow dynamical range. Consequently, the two relations are consistent with being drawn from a single underlying relation spanning the entire range from BCGs to clusters.

To estimate the difference in another common fitting method, we calculate the intrinsic scatter along the vertical direction (e.g., see Appendix A in Lelli et al. 2019). While performing the vertical MCMC method, we find a similar relation as $\log(M_{\rm bar}/M_\odot) = 3.9^{+0.1}_{-0.1}\log(\sigma_{\rm los}/{\rm km\ s^{-1}}) + 2.3^{+0.3}_{-0.3}$, albeit with a much larger lognormal intrinsic scatter $\sigma_{\rm int} = 40\% \pm 6\%$. Regardless of the scatter, the difference in the slope is negligible between the two methods.

3.2. Residuals

To examine the deviation of the dependence on some major properties of galaxies and clusters, we consider the orthogonal residuals after subtracting Equation (7) against four global quantities: baryonic mass, scale length ($R_{\rm e}$ for galaxies; r_{500} for clusters), surface density, and redshift in Figure 3. The residuals of all samples are distributed within a tiny range from -0.02 to 0.02 dex. Moreover, all diagrams display insignificant correlations with four galaxy-cluster properties, which is reminiscent of the BTFR for individual galaxies. Only the mass and velocity dispersion seem to matter. There is no obvious second parameter.

4. Discussions

For the first time, we reveal a tight empirical kinematic correlation, i.e., MVDR, on the BCG-cluster scale. The MVDR is a counterpart of a dynamical relation rather than a coincidence, which can be derived by the CLASH RAR (Tian et al. 2020). As

a new discovery of a strong correlation, the MVDR can provide a crucial test for the dark matter problem.

4.1. Consistency with the CLASH RAR

The CLASH RAR derives three implications of the kinematics in BCGs and clusters (Tian et al. 2020, 2021): (1) the flat velocity dispersion profile in BCGs; (2) the flat velocity dispersion profile in galaxy clusters; (3) the MVDR on the BCG-cluster scale as $\sigma^4 \propto GM_{\rm bar}g_\ddagger$. Initially, the implications in galaxy clusters were first confirmed in Tian et al. (2021) for (2) and partially (3), see Equation (3). Subsequently, our studies examine the rest of (1) and (3) in MaNGA BCGs and validate all the implications of the CLASH RAR. In addition, the MVDR on the BCG-cluster scale is identical to that in HIFLUGCS clusters, see Equations (7) and (3).

A larger acceleration scale also determines a smaller scale length $r_\ddagger$ of a flat velocity dispersion profile. In pressure supported systems, Milgrom (1984) defined a scale parameter as $r_\dagger = \sigma_{\rm los}^2 g_\dagger^{-1}$, for a flat velocity dispersion. When calculating with $g_\ddagger$ instead, we found $r_\ddagger = (0.4–4.1)$ kpc in MaNGA BCGs. Moreover, this scale is much smaller than a typical $R_{\rm e} \approx 30$ kpc (e.g., see Tian et al. 2020), which indicates a flat velocity dispersion even in the innermost region of BCGs.

Besides all the success of our results, one exception in our samples needs to be stressed. BCG "8943-9102" displays a declining profile and contributes the smallest velocity dispersion among the sample. This exception raises an interesting issue on BCGs: whether it appertains to a flat profile inherently.

4.2. Implications for Dark Matter Problems

The ΛCDM model implied the slope of three for the MVDR on the BCG-cluster scale, by assuming a constant baryon fraction (e.g., see Section 4.2 in Tian et al. 2021). According to their studies, the prediction in the ΛCDM model demonstrated

a discrepancy for smaller galaxy clusters. Coincidentally, MaNGA BCGs also disfavors the ΛCDM model with the same offset. On the contrary, the BFJR of elliptical galaxies were explained by adopting the abundance matching relation (e.g., see the discussions in Desmond & Wechsler 2017; Navarro et al. 2017). Regardless, the explanation still remains a mystery on the BCG-cluster scale.

MOND naturally explained the slope of four for the MVDR on the BCG-cluster scale, although a larger acceleration scale $g_{\ddagger}$ needs to be explained. One conceivable interpretation is the acceleration scale depending on the depth of the potential well (Zhao & Famaey 2012; Hodson & Zhao 2017). Besides, two characteristic scales could imply an underlying phase transition mechanism behind. Nevertheless, our discoveries provide a strict test for the attempts on the fundamental theory in MOND paradigm.

5. Summary

In the galactic systems, the acceleration scale $g_{\dagger}$ dominated in three empirical scaling relations: the RAR, the BTFR, and the BFJR. Among them, a tight dynamical relation, the RAR, can infer two kinematic counterparts of the BTFR and the BFJR, and vice versa. In addition, the acceleration scale $g_{\dagger}$ determined a scale distance $r_{\dagger}$ for a flat rotation curve and a flat velocity dispersion profile.

On the BCG-cluster scale, our studies filled the gap with such an empirical scaling relation, the MVDR, albeit with a larger acceleration scale $g_{\ddagger}$. The MVDR can be implied by the CLASH RAR as its kinematic relation, and vice versa. While investigating 54 MaNGA BCGs with IFU measurements, our works indicated a flat dispersion profile among all samples except one. Moreover, the flat tail can be determined by $r_{\ddagger}$ according to $g_{\ddagger}$.

In summary, the consistency between the CLASH RAR and the MVDR was confirmed by three different data sets: CLASH samples, HIFLUGCS clusters, and MaNGA BCGs. Both tight empirical correlations demonstrated tiny intrinsic scatters calculated by Bayesian statistics. Coincidentally, it raises an issue on such similarity between a galaxy and a cluster scale with two different acceleration scales: $g_{\dagger}$ and $g_{\ddagger}$, respectively. Nevertheless, the consistency of these relations provides a strict test for the dark matter problem.

ORCID iDs

Yong Tian ◉ https://orcid.org/0000-0001-9962-1816
Stacy S. McGaugh ◉ https://orcid.org/0000-0002-9762-0980
Chung-Ming Ko ◉ https://orcid.org/0000-0002-6459-4763
Yun-Hsin Hsu ◉ https://orcid.org/0000-0003-0381-562X

References

Aguado, D. S., Ahumada, R., Almeida, A., et al. 2019, ApJS, 240, 23
Bernardi, M., Hyde, J. B., Sheth, R. K., Miller, C. J., & Nichol, R. C. 2007, AJ, 133, 1741
Brouwer, M. M., Oman, K. A., Valentijn, E. A., et al. 2021, A&A, 650, A113
Bundy, K., Bershady, M. A., Law, D. R., et al. 2015, ApJ, 798, 7
Cherinka, B., Andrews, B. H., Sánchez-Gallego, J., et al. 2019, AJ, 158, 74
Chiu, I., Mohr, J. J., McDonald, M., et al. 2018, MNRAS, 478, 3072
Desmond, H., & Wechsler, R. H. 2017, MNRAS, 465, 820
Donahue, M., Voit, G. M., Mahdavi, A., et al. 2014, ApJ, 794, 136
Durazo, R., Hernandez, X., Cervantes Sodi, B., & Sanchez, S. F. 2018, ApJ, 863, 107
Famaey, B., & McGaugh, S. S. 2012, LRR, 15, 10
Foreman-Mackey, D., Farr, W., Sinha, M., et al. 2019, JOSS, 4, 1864
Foreman-Mackey, D., Hogg, D. W., Lang, D., & Goodman, J. 2013, PASP, 125, 306
Giodini, S., Pierini, D., Finoguenov, A., et al. 2009, ApJ, 703, 982
Hodson, A. O., & Zhao, H. 2017, A&A, 598, A127
Lelli, F., McGaugh, S. S., & Schombert, J. M. 2016, ApJL, 816, L14
Lelli, F., McGaugh, S. S., Schombert, J. M., Desmond, H., & Katz, H. 2019, MNRAS, 484, 3267
Lelli, F., McGaugh, S. S., Schombert, J. M., & Pawlowski, M. S. 2017, ApJ, 836, 152
McGaugh, S. S. 2011, PhRvL, 106, 121303
McGaugh, S. S. 2020, Galax, 8, 35
McGaugh, S. S., Lelli, F., & Schombert, J. M. 2016, PhRvL, 117, 201101
McGaugh, S. S., Schombert, J. M., Bothun, G. D., & de Blok, W. J. G. 2000, ApJL, 533, L99
Milgrom, M. 1983, ApJ, 270, 365
Milgrom, M. 1984, ApJ, 287, 571
Milgrom, M. 2020, SHPMP, 71, 170
Navarro, J. F., Benítez-Llambay, A., Fattahi, A., et al. 2017, MNRAS, 471, 1841
Oegerle, W. R., & Hoessel, J. G. 1991, ApJ, 375, 15
Postman, M., Coe, D., Benítez, N., et al. 2012, ApJS, 199, 25
Pradyumna, S., Gupta, S., Seeram, S., & Desai, S. 2021, PDU, 31, 100765
Samir, R. M., Takey, A., & Shaker, A. A. 2020, Ap&SS, 365, 142
Sanders, R. H. 1994, A&A, 284, L31
Sanders, R. H. 2003, MNRAS, 342, 901
Sanders, R. H. 2010, MNRAS, 407, 1128
Sartoris, B., Biviano, A., Rosati, P., et al. 2020, A&A, 637, A34
Tian, L., Hoekstra, H., & Zhao, H. 2009, MNRAS, 393, 885
Tian, Y., & Ko, C.-M. 2019, MNRAS, 488, L41
Tian, Y., Umetsu, K., Ko, C.-M., Donahue, M., & Chiu, I. N. 2020, ApJ, 896, 70
Tian, Y., Yu, P.-C., Li, P., McGaugh, S. S., & Ko, C.-M. 2021, ApJ, 910, 56
Umetsu, K., Zitrin, A., Gruen, D., et al. 2016, ApJ, 821, 116
Verheijen, M. A. W. 2001, ApJ, 563, 694
Yang, X., Mo, H. J., van den Bosch, F. C., et al. 2007, ApJ, 671, 153
Zaritsky, D., Gonzalez, A. H., & Zabludoff, A. I. 2006, ApJ, 638, 725
Zhang, Y. Y., Andernach, H., Caretta, C. A., et al. 2011, A&A, 526, A105
Zhao, H., & Famaey, B. 2012, PhRvD, 86, 067301